The SAMI Galaxy Survey: fossil group centrals are no more likely to be slow rotators

F. Scuccimarra [1], S.M. Croom [1,2], J. van de Sande [1,2,3], S. Barsanti [4,2], S. Brough [3,2], J.J. Bryant [1,2,5], L.C. Kimmig [6], C. del P. Lagos [7,2], R.-S. Remus [6], A. Ristea [7,2], S.M. Sweet [8,2] and S. Vaughan [1,2,9,10]

[1] Sydney Institute for Astronomy (SIfA), School of Physics, The University of Sydney, NSW 2006, Australia
[2] ARC Centre of Excellence for All Sky Astrophysics in 3 Dimensions (ASTRO 3D)
[3] School of Physics, University of New South Wales, NSW 2052, Australia
[4] Research School of Astronomy and Astrophysics, The Australian National University, Canberra, ACT 2611, Australia
[5] Astralis-USydney, School of Physics, The University of Sydney, NSW 2006, Australia
[6] Universitäts-Sternwarte München, Fakultät für Physik, Ludwig-Maximilians Universität, Scheinerstr. 1, D-81679 München, Germany
[7] International Centre for Radio Astronomy Research, University of Western Australia, Crawley, WA 6009, Australia
[8] School of Mathematics and Physics, University of Queensland, Brisbane, QLD 4072, Australia
[9] Astronomy, Astrophysics and Astrophotonics Research Centre, Macquarie University, Sydney, NSW 2109, Australia
[10] Centre for Astrophysics and Supercomputing, School of Science, Swinburne University of Technology, Hawthorn, VIC 3122, Australia
Author for correspondence: F. Scuccimarra, Email: fscu5535@uni.sydney.edu.au.

Abstract

Simulations suggest that slow rotating galaxies are the result of galaxy-galaxy mergers that have a tendency to randomise stellar orbits. The exact pathway for slow rotator formation, however, is still unclear. Our aim is to see whether there is a relationship between fossil groups – whose central galaxies are thought to have undergone more major merging than other central galaxies – and the stellar kinematic properties of those central galaxies. We classify all galaxy groups in the GAMA redshift survey whose central galaxies were observed with SAMI as: i) fossil groups, ii) mass gap groups (fossil-like groups), and iii) groups that are not dynamically evolved (NDEGs, i.e. controls). We compare the following properties of centrals across the three different group types: spin (λ_{Re}), the fraction of slow rotators (f_{SR}), and age. We also repeat our analysis on data from the EAGLE and Magneticum hydrodynamical cosmological simulations. In SAMI, we find that the spin parameter, slow rotator fraction, and age are broadly consistent across our three group types, i.e. the fossil groups, mass gap groups and NDEGs. We do find a weak indication that f_{SR} is slightly *lower* for fossil group centrals as compared to NDEG centrals. In contrast, in EAGLE and Magneticum, fossil and mass gap group centrals typically have a significantly lower λ_{Re} than NDEG centrals. Our results for SAMI suggest that the types of mergers that form fossil groups are not the types of mergers that form slow rotators. Merger count may be less important for slow rotator formation than specific merger conditions, such as the gas content of progenitors. *When* and *where* the merging occurs are also suspected to play an important role in slow rotator formation, and these conditions may differ for fossil group formation.

Keywords: galaxies: formation, galaxies: stellar kinematics, spin, slow rotators, fossil groups.

1. INTRODUCTION

Our understanding of the formation and evolution of galaxies steadily progresses as our ability to probe galaxies advances. Stellar kinematics provide unique insight into a galaxy's history and future, particularly when studied in conjunction with other galaxy properties such as environment, mass, and age. The rise of integral-field spectroscopy (IFS) surveys (e.g. SAURON (de Zeeuw et al., 2002); ATLAS^{3D} (Cappellari et al., 2011); CALIFA (Sánchez et al., 2012); SAMI (Croom et al., 2012); MANGA (Bundy et al., 2015)) over the past two decades has enabled two-dimensional stellar kinematic maps of galaxies to be determined, a significant improvement on traditional long-slit spectroscopy. The prevalence of available spatial information from IFS surveys has motivated the introduction of the spin parameter proxy λ_R by Emsellem et al. (2007): $\lambda_R \equiv \langle R|V| \rangle / \langle R\sqrt{V^2 + \sigma^2} \rangle$, quantifying the amount of ordered (V) to random (σ) stellar motion, where the radius R is typically the effective radius R_e.

λ_R, in conjunction with ellipticity, has consequently revealed a small, distinct population of dispersion-dominated *slow rotators* (SRs), in contrast to a rotationally-supported population of *fast rotators* (FRs) (Emsellem et al., 2007). Across all morphology types the fraction of slow rotators, $f_{SR} \lesssim 0.1$ (e.g. van de Sande et al., 2021b; Fraser-McKelvie & Cortese, 2022), whereas when only including early-types $f_{SR} \approx 0.15$ (Emsellem et al., 2011; Brough et al., 2017; van de Sande et al., 2021b). Indeed, SRs are predominantly *massive ellipticals*: observational studies have identified a strong correlation between f_{SR} and stellar mass, particularly above $M_* = 10^{11} M_\odot$ where $f_{SR} \approx 0.4$ (Emsellem et al., 2011; van de Sande et al., 2021b), with additional support from simulations (Lagos et al., 2018).

In our current picture of galaxy formation and evolution, galaxy-galaxy mergers are the primary means by which high mass ($M_* \gtrsim 10^{10.5} M_\odot$) galaxies accrete additional mass (e.g. Robotham et al., 2014). Early work suggests that ellipticals form via major merging (e.g. Toomre, 1977; Navarro & Benz, 1991; Hernquist, 1993). In addition, later work also suggests that multiple dry minor mergers are another pathway for elliptical formation (Naab et al., 2014; Moody et al., 2014; Schulze et al., 2018). This suggests that merging plays a key role in SR

formation.

Indeed, modelling by Khochfar et al. (2011) found that SRs have typically experienced more than twice as many major mergers than FRs. Binary merger simulations of disk galaxies by Bois et al. (2011) showed that minor disk-disk mergers almost always produced a fast rotator, whereas, major mergers in these simulations were able to produce both FRs and SRs. Simulations by Schulze et al. (2018) found that about half of the SRs are formed rapidly (in ~ 0.5 Gyr) through major mergers, while the other half have a different formation history not involving major mergers. Additionally, simulations have shown that the amount of gas involved in the merger appears to play a key role in the stellar kinematics of the remnant (e.g. Hoffman et al., 2010; Naab et al., 2014; Lagos et al., 2018, 2022). Gas-rich (wet) mergers were more likely to spin-up the merger remnant, due to the gas cooling and reforming a disk, with gas-poor (dry) mergers tending to have the opposite effect. Interestingly, Lagos et al. (2022) also found that about 15% of low mass ($M_* \lesssim 10^{10.5} M_\odot$) slow rotators in EAGLE formed without mergers.

The exact pathway to slow rotator formation, however, is still not fully understood. For instance, the relationship between environment and spin is tenuous. Several studies have detected a weak environmental trend with f_{SR} (e.g. Σ_3: Cappellari et al. 2011 and D'Eugenio et al. 2013; Σ_5: van de Sande et al. 2021a (fixed M_*); centrals vs satellites vs isolated galaxies: van de Sande et al. 2021a (fixed M_*) and Lagos et al. 2018 (simulations)). That is, SRs are more likely to exist in denser regions than sparser regions. Conversely, after controlling for stellar mass, other studies were unable to find a relationship with environment (centrals vs satellites: Greene et al. 2018; Σ_5: Brough et al. 2017; see also Veale et al. 2018 and Vaughan et al. 2024). To further complicate matters when studying spin and SR formation, the need for careful consideration of stellar population age has also recently become apparent (van de Sande et al., 2018; Croom et al., 2024; Rutherford et al., 2024).

A particular class of galaxy systems known as *fossil groups* (FGs; Ponman et al., 1994) are expected to have an extensive intra-group merger history. That is, most of the satellites have infallen via dynamical friction and merged with the central. These highly *dynamically evolved* systems are characterised by their low group multiplicity, a central that dominates the group in mass, and an X-ray emitting halo - typical of that of a much larger group or cluster (see Section 3.1 for more detail). Indeed, simulations suggest that, on average, FG centrals undergo more major mergers than non-FG centrals (Kundert et al., 2017). For a full review on the formation and evolution of fossil groups see Aguerri & Zarattini (2021).

The aim of our investigation is to further explore the merger hypothesis for slow rotator formation, focusing our attention on dynamically evolved groups. We wish to compare the stellar kinematic properties of the centrals of dynamically evolved groups to the centrals of groups that are not dynamically evolved. To this end, we make use of observational catalogue data from SAMI in conjunction with ancillary group data from GAMA (Driver et al., 2011), as well as data from

the EAGLE (Schaye et al., 2015; Crain et al., 2015; McAlpine et al., 2016) and Magneticum Pathfinder (Dolag et al., 2009a; Hirschmann et al., 2014) simulations (see Section 2 for more detail).

This paper is structured as follows. We describe the input data used in Section 2. In Section 3 we outline our approach to identifying fossil and mass gap groups. In Section 4 we present our findings regarding their stellar kinematic properties. We discuss our results in Section 5 and conclude in Section 6. Unless otherwise stated, we assume a cosmology with Ω_m = 0.3, Ω_Λ = 0.7 and H_0 = 70km s^{-1}Mpc^{-1}.

2. INPUT DATA

2.1 The GAMA Galaxy Survey

Commencing in 2008 and completing in 2014, the Galaxy And Mass Assembly (GAMA; Driver et al., 2011) survey combines multi-wavelength photometric data with a spectroscopic survey conducted with the 3.9 m Anglo-Australian Telescope (AAT) using the AAOmega multi-object spectrograph. As part of GAMA the AAT observed ≈ 300,000 galaxies over 286 deg^2, achieving a limiting magnitude $r_{AB} \approx 19.8$ mag and a completeness in excess of 98% in the equatorial regions.

We make use of GAMA data release 4 from the GAMA II survey (Baldry et al., 2018; Driver et al., 2022) in our investigation, for the three equatorial fields: G09, G12 and G15. In particular, we use the stellar mass, halo mass and group member identification data products.

About 40% of galaxies in GAMA are assigned to a particular galaxy group. Grouping is accomplished using a friends-of-friends grouping algorithm which was quality tested on a mock galaxy catalogue using the Millennium simulation (Springel et al., 2005). In essence, galaxies are linked based on both their projected and radial separations (see Robotham et al. 2011 for more detail).

Stellar mass estimates are based on stellar population synthesis modelling by Bruzual & Charlot (2003) (see Taylor et al., 2011, for more detail) and do not include flux scale corrections (which can add significant noise to the aperture based stellar mass estimates). Halo masses in GAMA were estimated based on the group velocity dispersion, σ, and the radius containing 50% of group members, R. That is, $M_{halo} = A\sigma^2 R$ to first order, where the scaling factor A = 10.0 was calibrated with simulations (Robotham et al., 2011). GAMA data is available at http://www.gama-survey.org/.

2.2 The SAMI Galaxy Survey

The SAMI Galaxy Survey (Croom et al., 2012) derives its name from the Sydney-AAO Multi-object Integral-Field Spectrograph, also installed on the AAT, which was used to observe about 3000 galaxies at low redshift ($z \lesssim 0.1$). About 75% of these galaxies come from the three equatorial regions of GAMA, providing a wealth of ancillary data for the SAMI catalogue, with the remaining galaxies selected from several cluster regions (Bryant et al., 2015; Owers et al., 2017).

The SAMI instrument consists of an array of 13 *hexabundles* (Bland-Hawthorn et al., 2011; Bryant et al., 2011, 2014), each
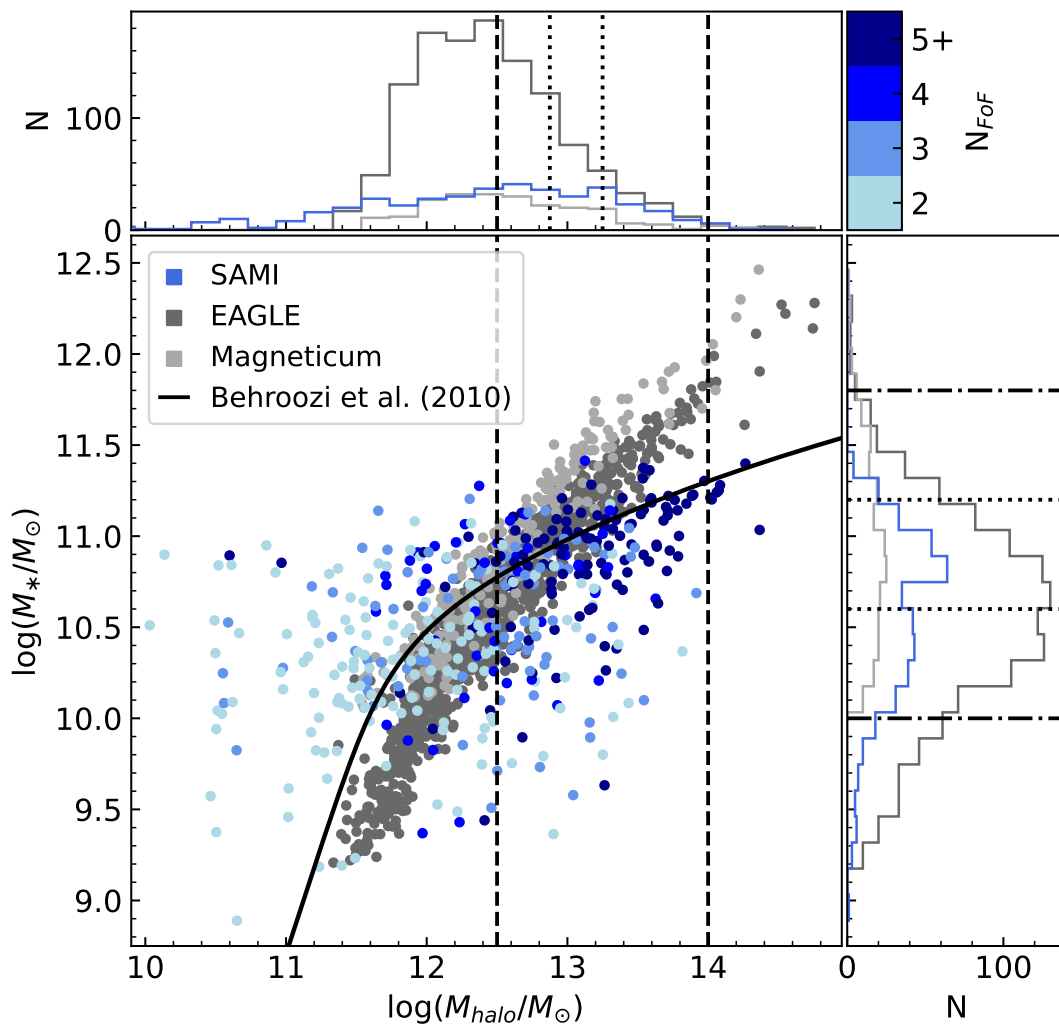
Figure 1. Central stellar mass vs. halo mass for the *full* group samples of SAMI (blue, good kinematic data for group central and no missing satellite stellar mass data only), EAGLE (dark grey), and Magneticum (light grey). A best-fit stellar mass - halo mass relation by Behroozi et al. (2010) is shown in solid black. Halo mass cuts are shown by the dashed lines, where our *final* SAMI, EAGLE, and Magneticum samples are contained within. Dotted lines demarcate the bins used when binning by stellar mass or halo mass. Dash-dotted lines are the minimum and maximum stellar mass bin boundaries, but are *not* a general cut on the full samples. Group multiplicity N_{FoF} is shown for SAMI (blue shades), indicating that most low halo mass groups are galaxy pairs whose halo masses are difficult to measure.

consisting of 61 optical fibres. With each hexabundle able to observe a different object, SAMI was capable of sampling a much greater number of galaxies in a given amount of time than its predecessors.

Reduction of SAMI data is performed primarily using the 2DF data reduction package (AAO software team, 2015) and the SAMI PYTHON package (Allen et al., 2014). For each observed galaxy, collected data is organised into cubes (Sharp et al., 2015; Scott et al., 2018) comprised of 50 x 50 spatial pixels (pixel side length 0.5 arcsec) and 2048 wavelengths. There are two primary data cubes for each galaxy corresponding to the blue (370–570nm) and red (630–740nm) wavelength ranges.

In our investigation we use stellar kinematic and (light-weighted) age data from SAMI data release 3 (Croom et al.,

2021). SAMI stellar kinematic measurements were performed using PENALIZED PIXEL-FITTING (pPXF) (Cappellari & Emsellem, 2004; Cappellari, 2017) (for more detail see van de Sande et al., 2017a). We use the λ_{Re} data that has been corrected for both seeing (Harborne et al., 2020) and aperture (van de Sande et al., 2017b) effects. R_e and ellipticity (ϵ) measurements were calculated using Multi Gaussian Expansion (MGE) fits (Emsellem et al., 1994; Cappellari, 2002). Vaughan et al. (2022) describe age measurements made for SAMI using stellar population synthesis modelling. SAMI catalogue data and documentation can be found at https://datacentral.org.au/.

2.3 EAGLE *simulations*

EAGLE (Evolution and Assembly of GaLaxies and their Environments; Schaye et al., 2015; Crain et al., 2015; McAlpine et al., 2016) is a collection of hydrodynamical simulations exploring supermassive black hole (BH) and galaxy formation in cosmologically representative volumes (25 to 100 comoving Mpc). EAGLE assumes the cosmological parameter values determined by Planck Collaboration XVI (Planck Collaboration et al., 2014): Ω_Λ = 0.693, Ω_m = 0.307, Ω_b = 0.04825, H_0 = 67.77 km s^{-1}Mpc^{-1}, and σ_8 = 0.8288. EAGLE employs sub-grid models for a range of physical processes including radiative cooling, stellar formation and evolution, BH gas accretion, and feedback. For a comprehensive discussion on EAGLE sub-grid physics see Crain et al. (2015).

Ref–L0100N1504 was the particular EAGLE simulation used in our investigation. Ref–L0100N1504 has a box side length of 100 comoving Mpc, 700 pc spatial resolution, consists of 2×1504^3 particles with an initial baryonic particle mass of $1.81 \times 10^6 M_\odot$ and a dark matter particle mass of $9.70 \times 10^6 M_\odot$ (McAlpine et al., 2016). A galaxy's stellar mass is taken to be the total star particle mass associated with the galaxy's subhalo within a 3D aperture of radius 30 proper kpc. In addition, feedback was calibrated to match the observed galaxy stellar mass function at z = 0 (Schaye et al., 2015).

We use the stellar kinematic measurements of EAGLE galaxies by Lagos et al. (2018), which were performed using a similar approach as in SAMI (van de Sande et al. 2017a; see also van de Sande et al. 2019). Briefly, Lagos et al. (2018) create two-dimensional stellar kinematic and luminosity maps for each galaxy with pixel width 1.5 proper kpc (c.f. 1.6 proper kpc at z = 0.05 for SAMI; van de Sande et al., 2017b). From these maps, *r*-band flux-weighted ellipticity (ϵ) and proxy spin parameter (λ_R) can then be determined. EAGLE data are publicly available and can be found at http://icc.dur.ac.uk/Eagle/database.php

2.4 MAGNETICUM PATHFINDER *simulations*

MAGNETICUM PATHFINDER (MAGNETICUM; Dolag et al., 2009a; Hirschmann et al., 2014) are another set of cosmological hydrodynamical simulations which were run using GADGET–3, an extension of GADGET–2 (Springel et al., 2005). MAGNETICUM adopts the Wilkinson Microwave Anisotropy Probe (Komatsu et al., 2011) cosmological parameters: Ω_Λ = 0.728, Ω_m = 0.272, Ω_b = 0.0451, H_0 = 70.4 km s^{-1}Mpc^{-1}, and σ_8 = 0.809. MAGNETICUM also incorporates a plethora of sub-grid physics including gas cooling and star formation (Springel & Hernquist, 2003), stellar and chemical evolution (Tornatore et al., 2007), magnetic fields (Dolag et al., 2009b), and black holes and AGN feedback (Springel et al., 2006; Fabjan et al., 2010; Hirschmann et al., 2014). For more details on this particular simulation, see also Teklu et al. (2015).

In this study we use galaxy catalogue data from snapshot 136 (z = 0.066) of the ultra high resolution 'Box4' simulation of MAGNETICUM. Box4 has a box side length of 68 comoving Mpc, initially 2×576^3 particles with dark matter particle mass $3.6 \times 10^7 M_\odot h^{-1}$ and gas particle initial mass

$7.3 \times 10^6 M_\odot h^{-1}$. Galaxies in MAGNETICUM were identified using SUBFIND (Springel et al., 2001), which includes the stellar halo of the group in the total stellar mass of the central.

We also use the Box4 stellar kinematic products measured by Schulze et al. (2018). These stellar kinematic measurements were performed using a similar procedure and spatial resolution to that used by Lagos et al. (2018) for EAGLE, except Schulze et al. (2018) use a mass-weighted approach and assume a constant mass-to-light ratio across each galaxy. MAGNETICUM data can be found at http://www.magneticum.org and at the web portal https://c2papcosmosim.uc.lrz.de/.

2.5 *Sample selection*

The full SAMI, EAGLE, and MAGNETICUM group samples in the central stellar mass–halo mass plane can be seen in Fig. 1. Our observational sample consists of galaxy groups in the equatorial GAMA fields (G09, G12, G15) for which there is reliable SAMI stellar kinematic data for the central – taken to be the most massive galaxy. Groups containing galaxies with missing stellar mass estimates are discarded to avoid potentially misleading mass gap calculations (see Section 3.1). For SAMI galaxies with repeat observations we choose the datacube pair with the higher signal-to-noise ratio that has been less affected by seeing conditions.

Since we identify dynamically evolved groups in our sample based on their mass gap and halo mass, we do not consider isolated galaxies in our investigation. It is perhaps possible that an isolated galaxy could be an *extreme* fossil group, where *all* of the satellites have merged with the central. However, we did not detect any isolated galaxies in our EAGLE or MAGNETICUM samples with a halo mass above our threshold for fossil groups. Hence, extreme fossil groups are likely exceedingly rare in the current epoch.

Fig. 1 reveals significant scatter in the stellar mass – halo mass plane for SAMI, largely due to measurement errors and uncertainties. In contrast, tight relations can be seen for EAGLE and MAGNETICUM. At the very high mass end, simulations also tend to add more stellar mass to the galaxy than observed. This is a problem of too many stars in EAGLE and MAGNETICUM, as well as these simulations adding all stripped stars to the central galaxy (Remus & Forbes, 2022). For a detailed comparison of dynamical properties between EAGLE, MAGNETICUM and SAMI, see van de Sande et al. 2019 who find the relationship between dynamical mass and stellar mass is broadly consistent between the data and simulations (e.g. their Fig. 6).

We restrict our analysis to galaxy groups with 12.5 < $\log(M_{halo}/M_\odot)$ < 14, for the following reasons. Firstly, van de Sande et al. (2021a) find that below this range, the halo mass function of the SAMI survey deviates considerably from simulation-based predictions by Angulo et al. (2012). Secondly, we found that our SAMI sample for $\log(M_{halo}/M_\odot)$ < 12.5 was dominated by galaxy pairs, whose halo masses are difficult to estimate and were hence contaminating our sample. Lastly, we impose the upper halo mass bound due to a statistically insignificant sample above this value. The number of galaxy

groups in our final SAMI, EAGLE, and Magneticum samples are 201, 501, and 115, respectively.

3. METHODS

3.1 Identifying dynamically evolved groups

A more formal definition for fossil groups than the qualitative description by Ponman et al. (1994) was proposed by Jones et al. (2003), based on the following two criteria:

1. $\Delta m_{12} \geq 2.0$ mag, where Δm_{12} is the difference in absolute magnitude in the r–band between the two brightest galaxies in the group.
2. $L_{X,bol} \geq 0.25 \times 10^{42}$ erg s^{-1}, where $L_{X,bol}$ is the bolometric X-ray luminosity in the 'soft' (0.5 – 2 keV) band. Gas is confined in the halo's potential, which depends on halo mass, and is consequently heated to the virial temperature (Ghirardini et al., 2019). In addition, halo mass is conserved under the merger process. Hence, galaxy groups with few members that are dominated by a single galaxy and are contained within a massive halo, typical of that of a much larger group/cluster, suggest an extensive merger history.

These two criteria are typically adopted in the literature as necessary and sufficient conditions for identifying fossil groups (e.g. D'Onghia et al., 2005; Dariush et al., 2007; Khosroshahi et al., 2004; Mendes de Oliveira et al., 2009; Zarattini et al., 2014). Some authors such as Kundert et al. (2017) used halo mass M_{halo} instead of $L_{X,bol}$. We will do the same in our approach to fossil group identification due to a lack of X-ray luminosity data for most of our sample. Therefore, the fossil groups identified in our study may not represent prototypical fossil groups identified by Jones et al. (2003) and others, but rather highly dynamically evolved systems. Additionally, some authors (e.g. Dariush et al., 2007) also explored systems that satisfy only the magnitude gap criterion, labelling them *optical fossil groups*, as weaker evidence for a dynamically evolved system. We adopt a similar approach in our investigation, except we refer to them as *mass gap groups*, since we use stellar mass in lieu of r–band magnitude. Finally, it is worth noting that the cut-off values for these conditions are somewhat arbitrary, by Jones et al. (2003)'s own admission.

3.1.1 Mass gap definition and threshold

As alluded to above, we take a stellar-mass-based approach to identifying dynamically evolved groups, i.e. mass gap groups and fossil groups. We define the mass gap of a group to be $\Delta m_{1\bar{2}\bar{3}}$: the difference between the most massive galaxy - the central - and the mean of the two most massive satellites, as it is less susceptible to scatter in the mass function than Δm_{12}. Indeed, some studies (e.g. Zhoolideh Haghighi et al., 2020) used Δm_{14} instead, with Aguerri & Zarattini (2021) arguing that it is a more reliable metric than Δm_{12}.

By fitting a curve to our sample in the stellar mass - luminosity plane, we find that Jones et al. (2003)'s magnitude gap threshold of 2.0 mag corresponds to a **mass gap threshold of 0.97 $\log(M_*/M_\odot)$.**

3.1.2 Determining the halo mass threshold

Given the lack of available X-ray luminosity data for our sample, we used halo mass estimates from GAMA in lieu of $L_{X,bol}$ and related the two quantities using a combination of two approaches. The first was based on work by Dariush et al. (2007) using data from the Millennium gas simulation (based on the Millennium simulation by Springel et al. 2005). Dariush et al. (2007) determined a relation between bolometric X-ray luminosity and dark matter halo mass, predicting a halo mass cut-off for fossil groups of $\sim$13.25 – 13.5 $\log(M_{halo}/M_\odot)$.

For the second approach we used the following observationally determined $L_x - M_{halo}$ relation by Bulbul et al. (2019) based on galaxy cluster data from the South Pole Telescope-Sunyaev-Zel'dovich survey (SPT-SZ; Bleem et al., 2015):

$$L_x = A_X \left(\frac{M_{halo}}{M_{piv}} \right)^{B_X} \left(\frac{E(z)}{E(z_{piv})} \right)^2 \left(\frac{1+z}{1+z_{piv}} \right)^{\gamma_x}$$

where $A_X = 4.15 \times 10^{44}$ erg s^{-1}, $B_X = 1.91$ and $\gamma_x = 0.252$ based on fits by Klein et al. (2022) for the eROSITA Final Equatorial Depth Survey (eFEDS; Brunner et al., 2022, which overlaps with the G09 GAMA region); $M_{piv} = 6.35 \times 10^{14} M_\odot$; $z_{piv} = 0.45$; $E(z) = \sqrt{\Omega_M (1+z)^3 + \Omega_\Lambda}$. We chose $z = 0.05$ based on the distribution of redshifts for galaxies in the SAMI catalogue (Croom et al., 2021). To convert from L_X to $L_{X,bol}$, we used eFEDS data (in the soft band, i.e. 0.5 – 2 keV) to find a linear relation for the two quantities. Consequently, we found that the threshold $L_{X,bol} = 0.25 \times 10^{42}$ erg s^{-1} corresponded to $L_X = 1.6 \times 10^{41}$ erg s^{-1}, and hence $\log(M_{halo}/M_\odot) = 13.13$.

The halo mass cuts determined using relations by Dariush et al. (2007) and Bulbul et al. (2019) slightly disagree, which is perhaps unsurprising given some of their differences: assumed cosmology, redshift range covered, and simulation vs observation study type, to name a few. A **halo mass threshold $\log(M_{halo}/M_\odot) \geq 13.25$** as a condition for a group to be considered a fossil group was ultimately selected as a good compromise. For comparison, Kundert et al. (2017) used a lower bound of $\log(M_{halo}/M_\odot) = 13.15$ in their fossil group study.

3.2 Slow rotator identification

For identifying slow rotating galaxies in the SAMI sample, we adopt the SAMI-optimised slow rotator selection criteria defined by van de Sande et al. (2021a):

$$\lambda_{Re} < \lambda_{Rstart} + \epsilon/4, \text{ with } \epsilon < 0.35 + \frac{\lambda_{Rstart}}{1.538}$$

where $\lambda_{Rstart} = 0.12$. Note that other (albeit qualitatively very similar) selection criteria do exist, e.g. $\lambda_{Re} < 0.1$ (Emsellem et al., 2007), $\lambda_{Re} < 0.31 \times \sqrt{\epsilon}$ (Emsellem et al., 2011) and $\lambda_{Re} < 0.08 + \epsilon/4$, $\epsilon < 0.4$ (Cappellari, 2016).

We only consider the fraction of slow rotators, f_{SR}, in our SAMI sample. We avoid identifying slow rotators in our EAGLE and Magneticum samples following van de Sande et al. (2021a)'s findings that SRs in simulations don't sit in
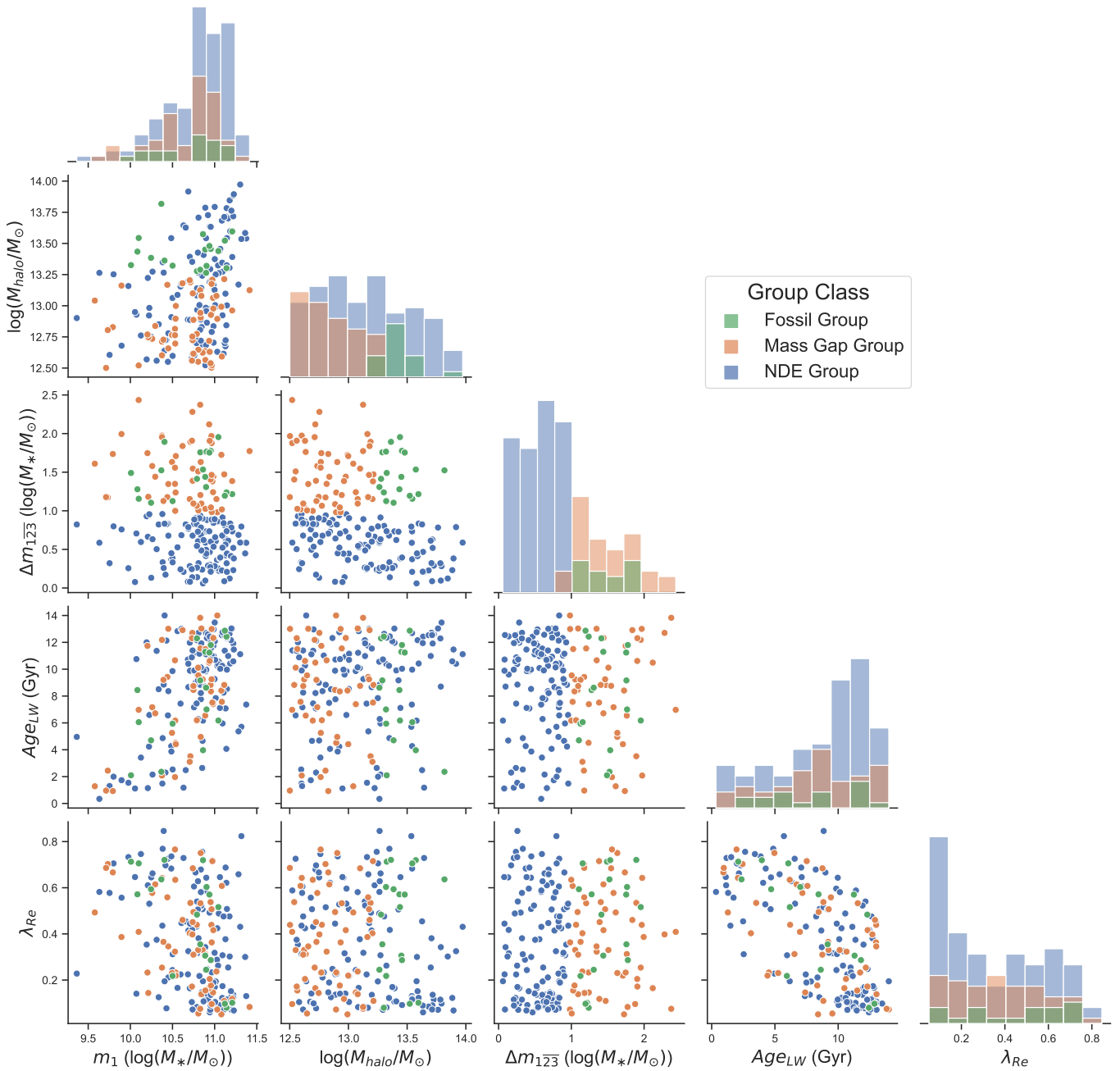
Figure 2. Relationships between key quantities, colour coded by group class, for our SAMI sample. Our selection criteria for group classification can be seen in the mass gap-halo mass plane. The central galaxies of dynamically evolved groups are fairly evenly distributed in λ_{Re} and light-weighted age. Conversely, central galaxies of the NDEGs appear more likely to have a lower spin and older age.

the same part of parameter space as SRs in observations. It is therefore difficult to define a uniform set of SR selection criteria, hence we look at average spin as well.

3.3 Bootstrapping and stellar mass matching

Bootstrapping (Efron, 1979) is a useful resampling technique when data is limited that allows one to estimate the underlying Probability Density Function (PDF) of the required

statistic. For each variable in our investigation, we take N random draws of the relevant sample (i.e. SAMI, EAGLE, or MAGNETICUM) with replacement, where N is the sample size, storing the mean of the resulting bootstrap sample. We then repeat this procedure for 10,000 iterations to generate a PDF for the desired statistic. We report the mean of each resulting PDF and the standard deviation of the bootstrap estimates of the mean is taken to be the uncertainty.

For quantities binned by halo mass, we utilise mass match-
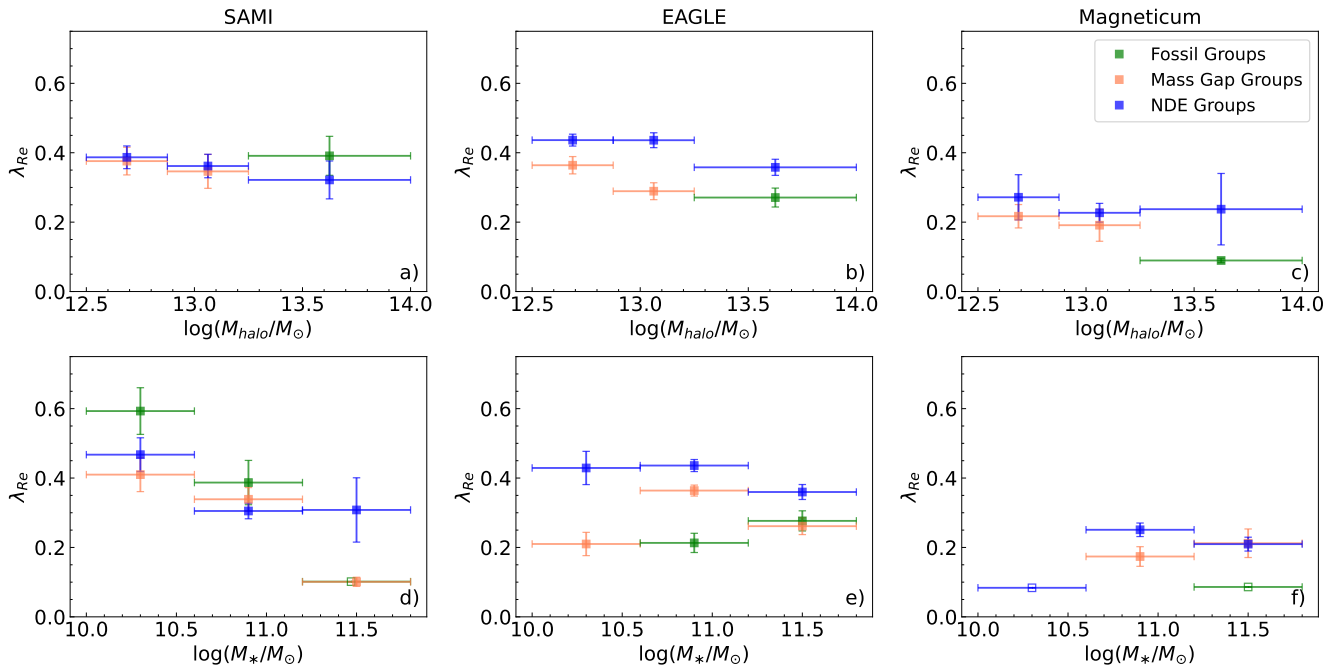
Figure 3. Group centrals in our SAMI (a, d), EAGLE (b, e), and Magneticum (c, f) data in the spin-halo mass (a, b, c) and spin-stellar mass (d, e, f) planes. In simulations, we see clear separation between the spins of DEG and NDEG centrals, supporting the idea that merging drives down λ_{Re}. In contrast, we find no significant difference for spin in SAMI between MGG and NDEG centrals, and we find that FG centrals have typically higher spins than NDEG centrals. Our SAMI results suggest that the mergers that form fossil groups are not the types of mergers that spin down galaxies and form slow rotators. Unfilled points do not have well-defined bootstrapping uncertainties as they contain only a single galaxy.

ing to avoid bias due to stellar mass, which we know is strongly correlated to λ_{Re} and f_{SR} (e.g. van de Sande et al., 2021b). Specifically, for each pair of halo mass bins, every central of a group that is not dynamically evolved has been mass matched within $0.15 \log(M_*/M_\odot)$ to a unique group central in the corresponding category (fossil group/mass gap group).

4. PROPERTIES OF FOSSIL AND MASS GAP GROUPS

4.1 Prevalence

The combined effect of the mass gap and halo mass cuts on our SAMI sample can be seen in the $\Delta m_{1\overline{23}} - \log(M_{halo}/M_\odot)$ plane of Fig. 2. Our SAMI sample was consequently divided into three distinct group classes (Table 1): *not dynamically evolved group* (NDEG) - galaxy groups with a mass gap below the threshold; *mass gap group* (MGG) - groups satisfying only the mass gap criterion; and *fossil group* (FG) - satisfying both the mass gap and halo mass criteria.

Table 1 also includes the incidences for the three group classes in our EAGLE and Magneticum samples. We consider the fraction of groups in each group class as it is more robust than number density, which is very sensitive to halo mass cut. We find similar fractions of FGs in both SAMI and EAGLE, but a lower fraction in Magneticum. MGGs (in lower mass haloes) are fractionally more common than FGs (in higher mass haloes) for both SAMI and EAGLE. The prevalence of MGGs in SAMI is slightly lower than in EAGLE, and substantially higher than in Magneticum. Indeed, our Magneticum sample consists

predominantly of groups that are not dynamically evolved.

It is difficult to compare incidence rates for fossil groups and mass gap groups across studies. This is largely due to differences in both the halo mass range considered and the satellite search radius adopted around the group central. Notwithstanding, a comparison of the literature is presented by Dariush et al. (2007, Table 1), which shows incidences broadly in line with our findings.

4.2 Group Class trends in SAMI

Fig. 2 reveals a number of general group class similarities and differences in our SAMI sample. First, the central galaxies of dynamically evolved groups (DEGs, i.e. FGs and MGGs) are fairly uniformly distributed in λ_{Re} and age. In contrast, centrals of NDEGs tend to be older (two-sample K-S test $p_{K-S} = 0.031$) and are overrepresented at very low spin (albeit not statistically significant: $p_{K-S} = 0.172$). This may be driven by the fact that the NDEGs have slightly higher mass, which is why we employ mass matching in our subsequent analysis. Second, NDEGs are distributed across the $12.5 < \log(M_{halo}/M_\odot) < 14$ halo mass range considered in our investigation, whereas DEGs are distributed up to $\log(M_{halo}/M_\odot) \approx 13.5$, beyond which we detect next to none ($p_{K-S} = 0.074$). Finally, we find that there are far fewer DEG centrals with $\log(M_*/M_\odot) \gtrsim 11$ relative to NDEG centrals ($p_{K-S} = 0.012$).
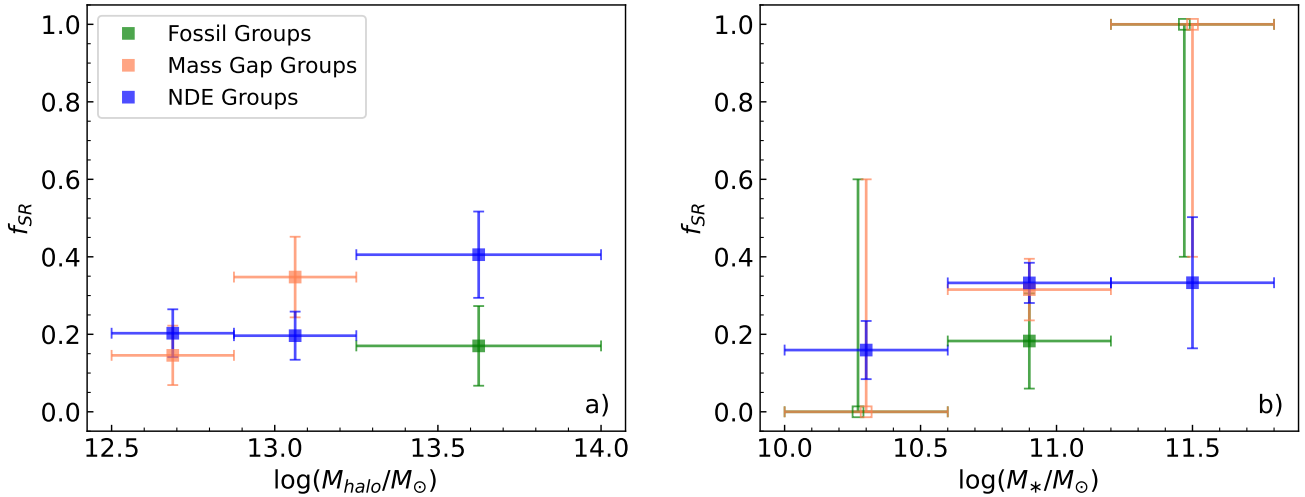
Figure 4. Our SAMI data in the fraction of slow rotators (f_{SR})-halo mass (a) and f_{SR}-stellar mass (b) planes. At fixed halo and stellar mass, FG centrals appear less likely to be slow rotators than NDEG centrals. These results directly follow from our findings in Fig. 3a and d given the slow rotator selection criteria we adopt (see Section 3.2). For unfilled points we report binomial uncertainties containing the 68% confidence regions, as they contain only a single galaxy.

Table 1. The number of groups for SAMI, EAGLE, and MAGNETICUM, in each group class category: fossil groups, mass gap groups, and groups that are not dynamically evolved (NDEG). NDEGs have been divided into high and low halo mass at the boundary of $\log(M_{halo}/M_{\odot}) = 13.25$. Numbers in parentheses are the fractions relative to the total number in each halo mass interval, with binomial uncertainties containing the 68% confidence regions (Cameron, 2011).

Group Class	Fossil Group	NDEG (high mass)	Mass Gap Group	NDEG (low mass)	Total
SAMI	19 ($0.27^{+0.06}_{-0.05}$)	51 ($0.73^{+0.05}_{-0.06}$)	58 ($0.44^{+0.04}_{-0.04}$)	73 ($0.56^{+0.04}_{-0.04}$)	201
EAGLE	33 ($0.34^{+0.05}_{-0.04}$)	64 ($0.66^{+0.04}_{-0.05}$)	215 ($0.53^{+0.02}_{-0.02}$)	189 ($0.47^{+0.02}_{-0.02}$)	501
MAGNETICUM	3 ($0.15^{+0.11}_{-0.05}$)	17 ($0.85^{+0.05}_{-0.11}$)	20 ($0.21^{+0.05}_{-0.04}$)	75 ($0.79^{+0.04}_{-0.05}$)	115

4.3 λ_{Re} and f_{SR}

Our results comparing the galaxy spin of centrals in FGs, MGGs, and NDEGs, in our observational and simulational data, are presented in Fig. 3. In Fig. 3a, b, and c we bin by halo mass in the following three bins: $12.5 < \log(M_{halo}/M_{\odot}) < 12.875$, $12.875 < \log(M_{halo}/M_{\odot}) < 13.25$, and $13.25 < \log(M_{halo}/M_{\odot}) < 14$. Data in Fig. 3d, e, and f have been binned by the stellar mass of the group central in three bins: $10 < \log(M_*/M_{\odot}) < 10.6$, $10.6 < \log(M_*/M_{\odot}) < 11.2$, and $11.2 < \log(M_{halo}/M_{\odot}) < 11.8$.

As discussed in Section 3.3, we emphasise the importance of controlling for stellar mass when comparing λ_{Re} between galaxies. When binning by *halo mass*, this was achieved by stellar mass matching unique DEG/NDEG central pairs in each bin to within $0.15\log(M_{halo}/M_{\odot})$. We do not employ this mass matching techinique when binning by *stellar mass* i.e. Fig. 3d, e, and f. Error bars indicate uncertainty on the mean at the 1σ level and are calculated using bootstrapping (see Section 3.3).

In SAMI, we find that for a given halo mass bin, the spins of NDEG centrals are comparable to those of MGG centrals. On the other hand, the spins of FG centrals are, on average, slightly higher (albeit not significantly) than their NDEG counterparts (Fig. 3a). Fig. 3d reveals that these higher λ_{Re} FG centrals

have a low or intermediate stellar mass. We find a similar result for f_{SR} (Fig. 4), that is, fossil group centrals are less likely to be slow rotators than NDEG centrals, driven by a population of fast rotator FG centrals in the low and intermediate stellar mass range. This is perhaps unsurprising given that the slow rotator selection criteria depends primarily on λ_{Re}. To be thorough, we repeated our analysis of f_{SR} using the other SR selection criteria stated in Section 3.2. We still found that FG centrals were slightly less likely to be SRs than NDEGs, however the difference seen in Fig. 4a between these two group classes was no longer significant.

These results for fossil group centrals are inconsistent with the current understanding of slow rotators. We know from simulations (e.g. Lagos et al., 2022; Valenzuela & Remus, 2022) as well as growing observational evidence (e.g. Rutherford et al., 2024) that mergers play a key role in the formation of slow rotators, and that fossil group centrals are thought to typically undergo more mergers than non-FG centrals (Kundert et al., 2017). Hence we would expect FG centrals to have a lower spin, on average, and be more likely to be slow rotators, than non-FG centrals. Our findings, however, suggest that the types of mergers that form fossil groups are not the types of mergers that form slow rotators.

In contrast, our λ_{Re} findings in EAGLE (Fig. 3b and e) and
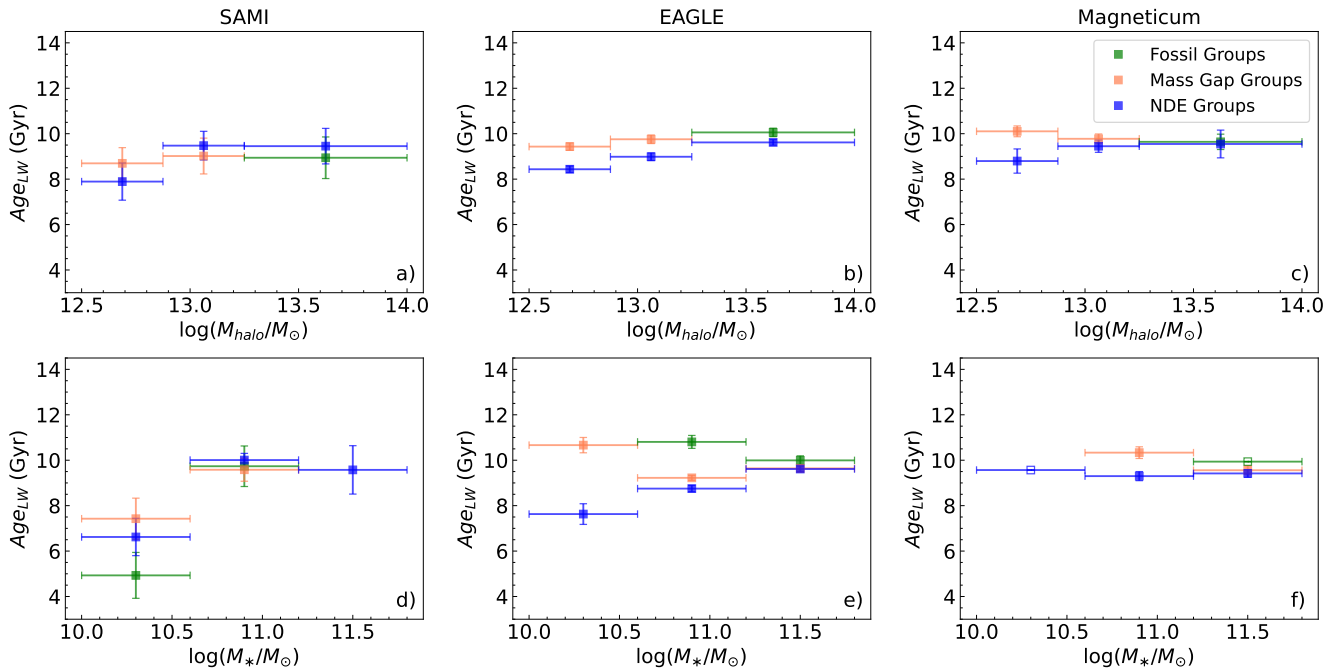
Figure 5. Similar to Fig. 3, but for light-weighted age, Age_{LW}. In SAMI, we detect no significant difference in Age_{LW} between DEG and NDEG centrals, except for a population of relatively younger, low mass FG centrals. In simulations, we detect a significant difference in age between NDEG and DEG centrals, in the low and intermediate halo and stellar mass bins.

MAGNETICUM (Fig. 3c and f) are in agreement with the current picture of slow rotator formation. Our results in simulations suggest that, at fixed halo/stellar mass, centrals in groups with a high mass gap ($\Delta m_{1\bar{2}3} \gtrsim 1$) tend to have a lower spin than centrals in low mass gap ($\Delta m_{1\bar{2}3} \lesssim 1$) groups. In most cases the difference in λ_{Re} in the simulations is striking: we detect a difference well beyond the 1σ level.

4.4 Light-weighted age

There is an emerging picture that λ_{Re} is most strongly correlated with age (van de Sande et al., 2018; Croom et al., 2024), that is, the spin of a galaxy decreases as the stellar population gets older. For instance, Croom et al. (2024) perform a partial correlation analysis and find that age is much more important than mass and environment in determining spin. This relationship is evident in the $\lambda_{Re} - Age_{LW}$ plane of Fig. 2.

We therefore perform an identical analysis for light-weighted age as for λ_{Re}, presented in Fig. 5. We use light-weighted age instead of mass-weighted age as spin is most likely related to when the galaxy is quenched (e.g. Lagos et al., 2018, 2022), making light-weighted age a better proxy for time since the significant star formation. In SAMI, for any given halo mass bin, we find no significant difference in age between DEG and NDEG centrals (Fig. 5a). When binning by stellar mass (Fig. 5d), however, we identify a population of low mass FG centrals that are generally younger than low mass MGG and NDEG centrals. We do not see a similar younger population of FG centrals in the intermediate and high mass bins. The same qualitative result is found when we

repeat the analysis with mass weighted ages (not shown).

In EAGLE and MAGNETICUM, we detect a significant difference in age between DEG and NDEG centrals, that is, DEG centrals tend to be older than NDEG centrals, in the low stellar mass and low halo mass regimes. This age gap generally decreases as we move to the intermediate bins, and is non-existent in the high stellar halo mass bins. Unlike in SAMI, we do *not* see a younger population of low mass FG centrals in simulations.

5. DISCUSSION

In SAMI, we find no difference in spin between FG centrals and NDEG centrals. Our observational results therefore suggest that the properties of mergers that spin down galaxies and form slow rotators are not the properties of mergers that form fossil groups. In contrast, our findings in EAGLE and MAGNETICUM strongly suggest that MGG and FG centrals have lower spins than NDEG centrals. We note that some small fraction of fossil groups may form with lower spins without the result of mergers, as is the case with SR formation Lagos et al. (2022). We will now discuss and provide possible explanations for these results.

5.1 Merger properties

Differences between the properties of mergers that are required to reduce galaxy spin and form a slow rotator, and the mergers that form fossil groups, may explain the λ_{Re} and f_{SR} discrepancies that we have found in SAMI. There is strong evidence from simulations that merger progenitors need to

be gas-poor or quenched, otherwise the gas will eventually reform a disk and hence spin-up the merger remnant (e.g. Hoffman et al., 2010; Naab et al., 2014; Lagos et al., 2018, 2022). Major merging tends to produce slow rotators with larger ellipticities (Khochfar et al., 2011; Bois et al., 2011; Jesseit et al., 2005; Schulze et al., 2018) whereas multiple dry minor mergers form most of the round slow rotators (Moody et al., 2014; Naab et al., 2014). Mergers with a small impact parameter, i.e. radial mergers have also been shown to be more effective at randomising stellar orbits and hence producing SRs (Duc et al., 2011; Karademir et al., 2019; Schulze et al., 2020).

In contrast, fossil group formation is essentially unaffected by such merger properties: merging of satellite galaxies with the group central is all that is required. This may explain why we found that fossil group centrals in SAMI were not more likely to be slow rotators than NDEG centrals. Further, since satellites are typically gas-rich disk galaxies, this might account for our FG centrals having a slightly higher average spin and lower f_{SR} than NDEG centrals.

So why do DEG centrals in EAGLE and MAGNETICUM have lower spins than NDEG centrals? We found that DEG centrals are slightly older in simulations (Fig. 5), so one possible explanation is that DEGs are more likely to contain passive galaxies. Another possibility is that the cold gas in satellites is stripped more efficiently by the hot group gas halo in simulations than in reality, which enhances the dry merging with the central galaxy.

5.2   *Merger remnants and redshift*

Most star formation in galaxies peaked around 10 Gyr ago and has since decreased substantially (Madau & Dickinson, 2014). Hence, mergers that occur at higher redshifts ($z \gtrsim 1$) tend to involve relatively younger galaxies, i.e. galaxies that are less likely to be quenched (Tacconi et al., 2010). Consequently, some studies have supported the notion that timing is important for reducing λ_{Re} and forming a slow rotator. Bezanson et al. (2018) found that quenched galaxies must lose spin in the $0 - 7$ Gyr range. Schulze et al. (2018) found that most fast-to-slow rotator evolution starts around 8 Gyr ago, although some formation before this time was also predicted in a larger simulation volume at redshifts as high as $z \approx 4$ (Kimmig et al., 2023). Lagos et al. (2022) instead found SR formation to preferentially occur around $2 - 6$ Gyr ago. Hence, whilst there is some range in timescales from different studies, most predict that slow rotators form between 8 Gyr ago and the present.

We therefore expect the remnants of mergers that occurred over 8 Gyr ago to be more likely to remain a rotating disk. Given that our SAMI results suggested that FG centrals are not more likely to be slow rotators than NDEG centrals, a plausible explanation is that the mergers that form fossil groups happen at higher redshifts. Chu et al. (2023) argue that fossil groups form before, and cease evolving by, $z \approx 1.8$ (10 Gyr ago), supporting this idea. Note that although for some of our observed FG centrals $Age_{LW} \approx 5$ Gyr (Fig. 5d), these galaxies may have undergone early merging and then continued to form stars.

5.3   *Location in large scale structure*

We are now starting to find evidence that some aspects of angular momentum in galaxies are related to large scale structure: the filaments, nodes and voids that make up the cosmic web (Barsanti et al., 2022). Whilst merging between the group central and satellites is required for a fossil system to form, if the group itself accretes new high mass galaxies - repopulates - then it may no longer be classified as a fossil group. This suggests that fossil groups are more likely to form in the underdense voids of the cosmic web. Indeed, Zarattini et al. (2023) found that fossil groups tend to be more isolated from large scale structure than non-fossil groups.

Slow rotators, on the other hand, may be more likely to form at nodes due to merging from different angles, i.e. along different filaments, having a particularly destructive effect on the remnant's spin. This possible difference in where slow rotators and fossil groups tend to form within the cosmic web may explain why we found that fossil group centrals in SAMI are not more likely to be slow rotators.

There are a couple of reasons as to why this location argument does not appear to hold in simulations. First, *when* the merging occurs may be more important than *where*. Second, the box sizes used in EAGLE and MAGNETICUM are perhaps too small to sample large scale structure with statistical significance. Moreover, box size has been shown to impact environment and structure formation (Kimmig et al., 2023).

5.4   *Measuring halo mass*

In our investigation we identified a population of low mass fossil group centrals in SAMI with a relatively higher λ_{Re} and lower Age_{LW} than low mass NDEG centrals. Specifically, these FG centrals have a stellar mass between $10^{10} M_{\odot}$ and $10^{10.6} M_{\odot}$, and a halo mass above $10^{13.25} M_{\odot}$, which is rather unusual. These galaxies lie in the bottom-right region of Fig. 1, far away from the tight $\log(M_*/M_{\odot}) - \log(M_{halo}/M_{\odot})$ relation seen in simulations. This suggests significant uncertainty in our halo mass measurements for fossil groups.

Our halo mass measurements for SAMI centrals were taken from GAMA, which were estimated by Robotham et al. (2011) using the following relation: $M_{halo} = A\sigma^2 R$, where σ is the group velocity dispersion, R is the radius containing 50% of the group's members, and $A = 10.0$ is a simulation-calibrated proportionality constant. We make the assumption that the halo mass of fossil groups follows the mean relation. There is a strong relationship between the shape of the halo mass probability density function and group multiplicity, since a greater number of galaxies yields more accurate estimates for R and especially σ. Robotham et al. (2011) find that bias is small for $N_{FoF} \geq 5$, however, for $N_{FoF} \leq 4$, the recovered distribution is not as tight and symmetrical (see Fig. 6 in Robotham et al., 2011).

Fig. 6 shows our SAMI sample in the $N_{FoF} - m_1$ plane, including the median (larger points) and 68% confidence interval of each stellar mass bin (demarcated by dashed lines). The group multiplicities of our dynamically evolved groups are in agreement with the literature (e.g. Jones et al., 2003; Dariush
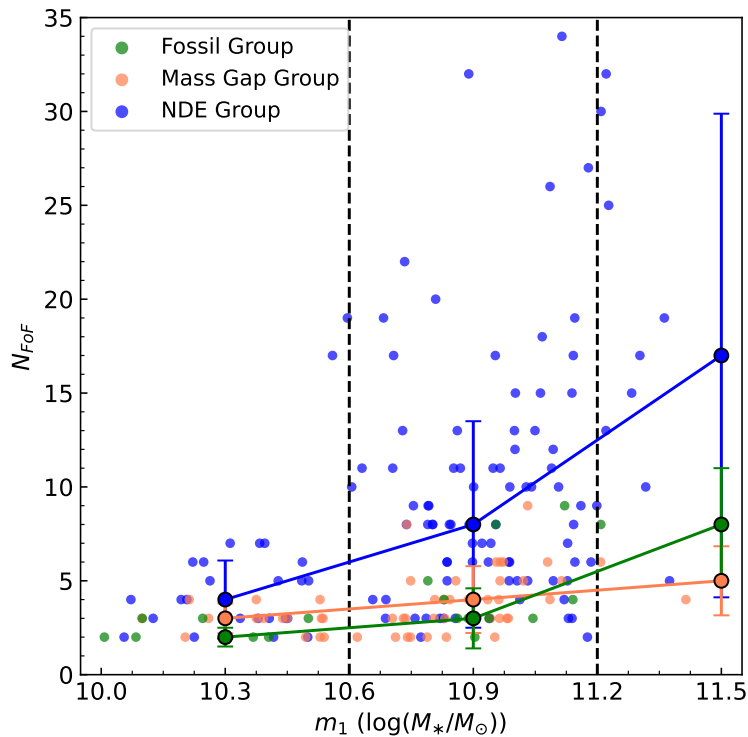
Figure 6. Group multiplicity (N_{FoF}) vs. central mass in our SAMI sample. Larger points are the median N_{FoF} of each stellar mass bin used in our investigation (delineated by dashed lines), with uncertainties as 68% confidence intervals. DEGs have very few group members in the low and intermediate mass ranges, making it difficult to estimate their halo mass. This is affecting our ability to distinguish between MGGs and FGs, adding noise.

et al., 2007), and are particularly low in the low and intermediate mass bins. Since FG and MGG classification differ only in halo mass, it is likely that our FG sample is being contaminated with MGGs, especially in the low mass bin, and that our MGG sample is being contaminated with FGs, particularly in the intermediate and high mass bins. This contamination may explain why we see an anomalous sub-population of low mass fossil group centrals, which is increasing the average spin and decreasing the average f_{SR} of the general FG population.

6. CONCLUSION

We have compared the spin parameter proxy λ_{Re}, light-weighted age (Age_{LW}), and fraction of slow rotators (f_{SR}) of SAMI Galaxy Survey centrals in groups at three different stages of dynamical evolution: not dynamically evolved (NDEGs), mass gap groups (MGGs), and fossil groups (FGs). We used a combination of mass gap and halo mass to classify SAMI centrals into our three group classes. We controlled for stellar mass throughout our investigation. We also repeated our analysis on samples from the EAGLE and Magneticum simulations, in the same halo mass range as for SAMI.

We find a clear λ_{Re} trend in simulations where MGG and FG centrals have lower spins, on average, than NDEG centrals. This trend persists whether we bin by halo mass or stellar mass. Given that FGs and MGGs typically undergo more merging than NDEGs, these findings support the current picture that

merging randomises stellar orbits and hence reduces galaxy spin.

In contrast, we do *not* see this trend in our SAMI sample. On average, SAMI FG centrals in the low and intermediate stellar mass range are found to have slightly higher spins than their NDEG central counterparts. Consequently, we find that SAMI FG centrals have a *lower* f_{SR} than SAMI NDEG centrals. These results suggest that the types of mergers that form the vast majority of fossil groups are not the types of mergers that form slow rotators.

Indeed, whilst slow rotator formation is necessarily a product of gas-poor or quenched progenitors, fossil group formation only requires satellite-central merging. Further, there is evidence to suggest that SRs generally form later than FGs ($\lesssim 8$ Gyr ago vs. ≈ 10 Gyr ago, respectively). SRs and FGs may also preferentially form in different locations in large scale structure: SRs at nodes to more effectively reduce angular momentum and FGs in voids to avoid becoming repopulated. Finally, we suspect uncertainty in halo mass measurements to be introducing significant noise to MGGs and FGs in our SAMI sample.

For Age_{LW}, we detected a population of relatively younger low mass FG centrals in SAMI that was not present in our EAGLE and Magneticum data. We otherwise found no significant difference in age between DEG and NDEG centrals in SAMI. Conversely, in simulations, DEG centrals were gen-

erally slightly older than NDEG centrals, in the low and intermediate stellar and halo mass regimes.

The Hector galaxy survey (Bryant et al., 2020) – the successor of SAMI – will provide a larger data set (roughly 5× larger) to better understand the relationship between dynamically evolved groups and slow rotators. Additionally, the full eROSITA All-Sky Survey (Predehl et al., 2021) will provide X-ray data needed to more reliably identify fossil groups, and also enable the identification of isolated fossil groups where all of the satellites have merged with the central. Finally, higher redshift stellar kinematic data, which could be obtained with the James Webb Space Telescope NIRSpec instrument (Gardner et al., 2006), would shed more light on when SRs form.

Data Availability Statement
Data used in this investigation are available upon reasonable request. See Section 2 for accessing publicly available GAMA, SAMI, EAGLE, and MAGNETICUM data.

References

AAO software team. 2015, 2dfdr: Data reduction software, Astrophysics Source Code Library, record ascl:1505.015, ascl:1505.015

Aguerri, J. A. L., & Zarattini, S. 2021, Universe, 7, 132

Allen, J. T., Green, A. W., Fogarty, L. M. R., et al. 2014, SAMI: Sydney-AAO Multi-object Integral field spectrograph pipeline, Astrophysics Source Code Library, record ascl:1407.006, ascl:1407.006

Angulo, R. E., Springel, V., White, S. D. M., et al. 2012, MNRAS, 426, 2046

Baldry, I. K., Liske, J., Brown, M. J. I., et al. 2018, MNRAS, 474, 3875

Barsanti, S., Colless, M., Welker, C., et al. 2022, MNRAS, 516, 3569

Behroozi, P. S., Conroy, C., & Wechsler, R. H. 2010, ApJ, 717, 379

Bezanson, R., van der Wel, A., Pacifici, C., et al. 2018, ApJ, 858, 60

Bland-Hawthorn, J., Bryant, J., Robertson, G., et al. 2011, Optics Express, 19, 2649

Bleem, L. E., Stalder, B., de Haan, T., et al. 2015, ApJS, 216, 27

Bois, M., Emsellem, E., Bournaud, F., et al. 2011, MNRAS, 416, 1654

Brough, S., van de Sande, J., Owers, M. S., et al. 2017, ApJ, 844, 59

Brunner, H., Liu, T., Lamer, G., et al. 2022, A&A, 661, A1

Bruzual, G., & Charlot, S. 2003, MNRAS, 344, 1000

Bryant, J. J., Bland-Hawthorn, J., Fogarty, L. M. R., Lawrence, J. S., & Croom, S. M. 2014, MNRAS, 438, 869

Bryant, J. J., O'Byrne, J. W., Bland-Hawthorn, J., & Leon-Saval, S. G. 2011, MNRAS, 415, 2173

Bryant, J. J., Owers, M. S., Robotham, A. S. G., et al. 2015, MNRAS, 447, 2857

Bryant, J. J., Bland-Hawthorn, J., Lawrence, J., et al. 2020, in Society of Photo-Optical Instrumentation Engineers (SPIE) Conference Series, Vol. 11447, Society of Photo-Optical Instrumentation Engineers (SPIE) Conference Series, 1144715

Bulbul, E., Chiu, I. N., Mohr, J. J., et al. 2019, ApJ, 871, 50

Bundy, K., Bershady, M. A., Law, D. R., et al. 2015, ApJ, 798, 7

Cameron, E. 2011, PASA, 28, 128

Cappellari, M. 2002, MNRAS, 333, 400

—. 2016, ARA&A, 54, 597

—. 2017, MNRAS, 466, 798

Cappellari, M., & Emsellem, E. 2004, PASP, 116, 138

Cappellari, M., Emsellem, E., Krajnović, D., et al. 2011, MNRAS, 413, 813

Chu, A., Durret, F., Ellien, A., et al. 2023, arXiv e-prints, arXiv:2303.05146

Crain, R. A., Schaye, J., Bower, R. G., et al. 2015, MNRAS, 450, 1937

Croom, S. M., Lawrence, J. S., Bland-Hawthorn, J., et al. 2012, MNRAS, 421, 872

Croom, S. M., Owers, M. S., Scott, N., et al. 2021, MNRAS, 505, 991

Croom, S. M., van de Sande, J., Vaughan, S. P., et al. 2024, MNRAS, 529, 3446

Dariush, A., Khosroshahi, H. G., Ponman, T. J., et al. 2007, MNRAS, 382, 433

de Zeeuw, P. T., Bureau, M., Emsellem, E., et al. 2002, MNRAS, 329, 513

D'Eugenio, F., Houghton, R. C. W., Davies, R. L., & Dalla Bontà, E. 2013, MNRAS, 429, 1258

Dolag, K., Borgani, S., Murante, G., & Springel, V. 2009a, MNRAS, 399, 497

Dolag, K., Stasyszyn, F., Donnert, J., & Pakmor, R. 2009b, in Cosmic Magnetic Fields: From Planets, to Stars and Galaxies, ed. K. G. Strassmeier, A. G. Kosovichev, & J. E. Beckman, Vol. 259, 519–528

D'Onghia, E., Sommer-Larsen, J., Romeo, A. D., et al. 2005, ApJ, 630, L109

Driver, S. P., Hill, D. T., Kelvin, L. S., et al. 2011, MNRAS, 413, 971

Driver, S. P., Bellstedt, S., Robotham, A. S. G., et al. 2022, MNRAS, 513, 439

Duc, P.-A., Cuillandre, J.-C., Serra, P., et al. 2011, MNRAS, 417, 863

Efron, B. 1979, The Annals of Statistics, 7, 1

Emsellem, E., Monnet, G., Bacon, R., & Nieto, J. L. 1994, A&A, 285, 739

Emsellem, E., Cappellari, M., Krajnović, D., et al. 2007, MNRAS, 379, 401

—. 2011, MNRAS, 414, 888

Fabjan, D., Borgani, S., Tornatore, L., et al. 2010, MNRAS, 401, 1670

Fraser-McKelvie, A., & Cortese, L. 2022, ApJ, 937, 117

Gardner, J. P., Mather, J. C., Clampin, M., et al. 2006, Space Sci. Rev., 123, 485

Ghirardini, V., Eckert, D., Ettori, S., et al. 2019, A&A, 621, A41

Greene, J. E., Leauthaud, A., Emsellem, E., et al. 2018, ApJ, 852, 36

Harborne, K. E., van de Sande, J., Cortese, L., et al. 2020, MNRAS, 497, 2018

Hernquist, L. 1993, ApJ, 409, 548

Hirschmann, M., Dolag, K., Saro, A., et al. 2014, MNRAS, 442, 2304

Hoffman, L., Cox, T. J., Dutta, S., & Hernquist, L. 2010, ApJ, 723, 818

Jesseit, R., Naab, T., & Burkert, A. 2005, MNRAS, 360, 1185

Jones, L. R., Ponman, T. J., Horton, A., et al. 2003, MNRAS, 343, 627

Karademir, G. S., Remus, R.-S., Burkert, A., et al. 2019, MNRAS, 487, 318

Khochfar, S., Emsellem, E., Serra, P., et al. 2011, MNRAS, 417, 845

Khosroshahi, H. G., Jones, L. R., & Ponman, T. J. 2004, MNRAS, 349, 1240

Kimmig, L. C., Remus, R.-S., Seidel, B., et al. 2023, arXiv e-prints, arXiv:2310.16085

Klein, M., Oguri, M., Mohr, J. J., et al. 2022, A&A, 661, A4

Komatsu, E., Smith, K. M., Dunkley, J., et al. 2011, ApJS, 192, 18

Kundert, A., D'Onghia, E., & Aguerri, J. A. L. 2017, ApJ, 845, 45

Lagos, C. d. P., Emsellem, E., van de Sande, J., et al. 2022, MNRAS, 509, 4372

Lagos, C. d. P., Schaye, J., Bahé, Y., et al. 2018, MNRAS, 476, 4327

Madau, P., & Dickinson, M. 2014, ARA&A, 52, 415

McAlpine, S., Helly, J. C., Schaller, M., et al. 2016, Astronomy and Computing, 15, 72

Mendes de Oliveira, C. L., Cypriano, E. S., Dupke, R. A., & Sodré, Laerte, J. 2009, AJ, 138, 502

Moody, C. E., Romanowsky, A. J., Cox, T. J., Novak, G. S., & Primack, J. R. 2014, MNRAS, 444, 1475

Naab, T., Oser, L., Emsellem, E., et al. 2014, MNRAS, 444, 3357

Navarro, J. F., & Benz, W. 1991, ApJ, 380, 320

Owers, M. S., Allen, J. T., Baldry, I., et al. 2017, MNRAS, 468, 1824

Planck Collaboration, Ade, P. A. R., Aghanim, N., et al. 2014, A&A, 571, A16

Ponman, T. J., Allan, D. J., Jones, L. R., et al. 1994, Nature, 369, 462

Predehl, P., Andritschke, R., Arefiev, V., et al. 2021, A&A, 647, A1

Remus, R.-S., & Forbes, D. A. 2022, ApJ, 935, 37

Robotham, A. S. G., Norberg, P., Driver, S. P., et al. 2011, MNRAS, 416, 2640

Robotham, A. S. G., Driver, S. P., Davies, L. J. M., et al. 2014, MNRAS, 444, 3986

Rutherford, T. H., van de Sande, J., Croom, S. M., et al. 2024, MNRAS, 529, 810

Sánchez, S. F., Kennicutt, R. C., Gil de Paz, A., et al. 2012, A&A, 538, A8

Schaye, J., Crain, R. A., Bower, R. G., et al. 2015, MNRAS, 446, 521

Schulze, F., Remus, R.-S., Dolag, K., et al. 2020, MNRAS, 493, 3778

—. 2018, MNRAS, 480, 4636

Scott, N., van de Sande, J., Croom, S. M., et al. 2018, MNRAS, 481, 2299

Sharp, R., Allen, J. T., Fogarty, L. M. R., et al. 2015, MNRAS, 446, 1551

Springel, V., Frenk, C. S., & White, S. D. M. 2006, Nature, 440, 1137

Springel, V., & Hernquist, L. 2003, MNRAS, 339, 289

Springel, V., White, S. D. M., Tormen, G., & Kauffmann, G. 2001, MNRAS, 328, 726

Springel, V., White, S. D. M., Jenkins, A., et al. 2005, Nature, 435, 629

Tacconi, L. J., Genzel, R., Neri, R., et al. 2010, Nature, 463, 781

Taylor, E. N., Hopkins, A. M., Baldry, I. K., et al. 2011, MNRAS, 418, 1587

Teklu, A. F., Remus, R.-S., Dolag, K., et al. 2015, ApJ, 812, 29

Toomre, A. 1977, in Evolution of Galaxies and Stellar Populations, ed. B. M. Tinsley & D. C. Larson, Richard B. Gehret, 401

Tornatore, L., Borgani, S., Dolag, K., & Matteucci, F. 2007, MNRAS, 382, 1050

Valenzuela, L. M., & Remus, R.-S. 2022, arXiv e-prints, arXiv:2208.08443

van de Sande, J., Bland-Hawthorn, J., Brough, S., et al. 2017a, MNRAS, 472, 1272

van de Sande, J., Bland-Hawthorn, J., Fogarty, L. M. R., et al. 2017b, VizieR Online Data Catalog, J/ApJ/835/104

van de Sande, J., Scott, N., Bland-Hawthorn, J., et al. 2018, Nature Astronomy, 2, 483

van de Sande, J., Lagos, C. D. P., Welker, C., et al. 2019, MNRAS, 484, 869

van de Sande, J., Vaughan, S. P., Cortese, L., et al. 2021a, MNRAS, 505, 3078

van de Sande, J., Croom, S. M., Bland-Hawthorn, J., et al. 2021b, MNRAS, 508, 2307

Vaughan, S. P., Barone, T. M., Croom, S. M., et al. 2022, MNRAS, 516, 2971

Vaughan, S. P., van de Sande, J., Fraser-McKelvie, A., et al. 2024, MNRAS, 528, 5852

Veale, M., Ma, C.-P., Greene, J. E., et al. 2018, MNRAS, 473, 5446

Zarattini, S., Aguerri, J. A. L., Tarrío, P., & Corsini, E. M. 2023, A&A, 676, A133

Zarattini, S., Barrena, R., Girardi, M., et al. 2014, A&A, 565, A116

Zhoolideh Haghighi, M. H., Raouf, M., Khosroshahi, H. G., Farhang, A., & Gozaliasl, G. 2020, ApJ, 904, 36